Trabajo de Fin de Grado de Física

Electrodinámica Cuántica en Cavidad Multimodo

Jesús Matías alcaine Cuervo

Directores:

David Zueco Láinez

Fernando Luis Vitalla

Departamento de Física de la Materia Condensada

Facultad de Ciencias, Universidad de Zaragoza

Junio de 2022

Undergraduate Dissertation in Physics

Multimode Cavity QED

Jesús Matías Alcaine Cuervo

Directors:

David Zueco Láinez

Fernando Luis Vitalla

Department of Condensed Matter Physics

Faculty of Science, University of Zaragoza

June 2022

I would like to dedicate a few lines to briefly thank my family and closest friends, for their unconditional love and support and for always helping me along this journey that has been the Physics degree. I would also like to thank my classmates, without whom these four years would not have been the same.

And finally, with regard to this Undergraduate Dissertation, I would like to thank David for his closeness and stimulating lessons, as well as Juan and Sergi for their patience and support throughout so many moments in front of the screen. All of you have been everything and more than I could have hoped for in this project.

Contents

.

Introduction

The field of Quantum Technologies has received ever growing interest in the past decades. Even though many currently widespread technologies, such as lasing, nuclear magnetic resonance, LED screens or semiconductor processors find their origin in quantum theory, they are not typically considered under the umbrella term of Quantum Technologies. Instead, the term is reserved for a number of promising applications that are in development, namely in the fields of quantum computation and simulation, quantum communications and cryptography and quantum metrology [1]. Whether the scientific community will deliver on its promises depends on our ability to model and control the different quantum systems that underlie these technologies. This poses serious theoretical and experimental challenges that constitute the state-of-the-art of current research in the field. Theoretical because only a few of these systems can be solved analytically, or numerically, and experimental because precisely tunable large quantum systems are fragile in nature.

One of the main building blocks of these quantum technologies is the qubit. In order to probe and control a qubit without decoherence, it is often coupled to an electromagnetic cavity. The light-matter interactions that arise from such a system give rise to the field of cavity quantum electrodynamics (QED) [2]. The central parameter governing the behaviour of these systems is the coupling between the qubit and the cavity. The achievement of strong coupling marked a milestone of the field, opening the possibility of entangling light and matter. The coupling is defined as strong when the qubit and cavity losses are negligible in comparison. The development of circuit QED, where cavities and qubits are realized out of superconducting circuits, has allowed us to reach even stronger regimes of coupling, such as ultrastrong and deep strong coupling [3].

Like in all fields of physics, the theoretical development of cavity QED has relied on several toy models that deliver an approximate description of a cavity and qubit system. These toy models are desinged to be analytically tractable while capturing the main features of the system they seek to describe. In this regard, the Rabi model stands out in the field of cavity QED. It describes a two level system (the qubit) coupled to a single bosonic mode (the cavity) [4]. However, as the field matures, it becomes necessary to develop more nuanced models that capture the non-ideal features of true experimental systems. Once such feature is the presence of more than one electromagnetic mode in the cavity. In this undergraduate dissertation, we extend the Rabi model to accomodate several bosonic modes, arriving at the spin-boson model. Additionally, we also account for the possibility of a bias field acting on the two-level system. Accordingly, we also generalize the analytical tools typically used to study the Rabi model to the multimode case. We employ a generalized polaron transform, which is a variational *ansatz* that allows us to tackle the full coupling spectrum, from weak to deep strong coupling [5]. We compare this generalized polaron ansatz against the standard one and validate it using exact diagonalization of the system.

Objectives and outline

Several objectives were set out at the beginning of this work. First, we aimed to review and understand the basic single-atom cavity QED models, including the quantum Rabi and Jaynes-Cummings, as well as the approximations commonly used in their treatment. We also wanted to analyse their basic phenomenology and the different regimes they exhibit depending on the coupling strength between light and matter. Furthermore, we sought to identify the biased multimode Rabi, i.e. the biased spin-boson model, as a generalisation of the standard one. Our goal also was to establish that cavity QED implementations are many-body systems that are difficult to handle both analytically and numerically, and to understand the polaron transform as a tool to treat these models semi-analytically, proceeding afterwards to apply a generalisation of it to the mentioned biased spin-boson. With that, we would be able to study its phenomenology and compare our generalised polaron transform with the original. Further, we also sought to validate our results against exact diagonalisation and draw the relevant conclusions.

In accordance with the above, this Undergraduate Dissertation is structured as follows: In Section 1, we present and give an in depth review of the quantum Rabi model, we set the scene of possible coupling regimes and motivate the polaron transform. We also include a microscopic derivation of it. In Section 2 we proceed with the introduction of the standard polaron transform, as well as our calculations for a biased spin-boson model using a newly proposed polaron ansatz, arriving at the end to the transformed Hamiltonian and computing the ground state energy. Then in Section 3 we study the phenomenology of the aforementioned biased spin-boson model via different observables using the previous calculations. We close off by validating our results with a comparison with the exact diagonalization of the Hamiltonian. We are mindful of the influence of increasing the number of modes M versus the single mode case. Finally, we draw some conclusions. Some technical details are included in the appendices, which contain complementary calculations, as well as a link to a repository where all the code for numerical calculations needed in this work can be found.

1 Cavity QED

1.1 Quantum Rabi model and coupling regimes

Quantum electrodynamics (QED) deals with both radiation and matter within quantum mechanics principles, and consequently treats the interactions between them in terms of photons, that is, light quanta. Specifically, in this work they will be treated in the non relativistic limit of the theory, which is the area of influence belonging to quantum Optics. Electromagnetic fields are now treated as quantum operators acting on field state vectors, and atoms on their behalf serve as elements with different levels of quantized energy.

Here we treat the case of atoms confined in a reflective cavity or photonic resonator, so that if the atom is excited and emits a photon, this is ultimately reabsorbed obtaining a periodic or coherent coupling, unlike the contrasting case of free space where the photon is emitted in an irreversible process. Cavity QED [2] indeed comprises the collection of atoms interacting with cavity photons, whose representative view is illustrated in Fig. 1. Diving slightly more into the topic, the finite volume of the cavity selects the allowed wavelengths for the photons, and restricts the atom EM frequencies to the ones corresponding to stationary waves, these are $\omega_n = c\pi n/L$. Furthermore, the atom is mostly projected in a two level system (TLS) with energy difference Δ, assuming only two states are relevant in its dynamics.

Now, in the case where the light-matter coupling is weak enough, the atom primarily couples to the mode closest to the atom level spacing $\omega_n = \omega_c \approx \Delta$, yielding the most paradigmatic Hamiltonian in Cavity QED,

$$\mathcal{H}_{qR} = \frac{\Delta}{2}\sigma^x + \omega_c a_k^\dagger a_k + g\sigma^z \left(a_k^\dagger + a_k\right), \tag{1}$$

the quantum Rabi model. The three terms correspond to the TLS, with Δ being the atom level spacing or the bare frequency, then the bosonic term with the energy of the selected mode ω_c, and finally the coupling between the TLS and the cavity, which is tuned by the coupling strength g.

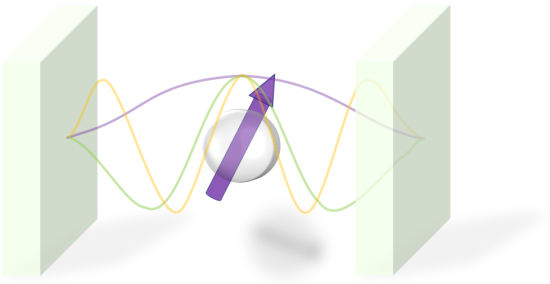

Fig. 1: Schematic view of a TLS embedded in a 1D Cavity.

The dominant parameter in the system is indeed the coupling strength g, usually expressed in terms of the modal frequency ω_c as the normalized coupling strength g/ω_c [3]. In the following, we will discuss in terms of the normalized coupling. Several regimes of behaviour are observed by studying the latter model (1) for increasing values of the coupling.

First, for a *weak coupling regime* (WC), corresponding to $g/\omega_c \ll 1$, the Rabi model (1) can be approximated by the Jaynes-Cummings model using the Rotating Wave Aproximation (RWA), which eliminates the so called counter-rotating parts of the interaction term leaving thus

$$\mathcal{H}_{qR} \equiv \mathcal{H}_{JC} = \frac{\Delta}{2}\sigma^x + \omega_c a_k^\dagger a_k + g\left(\sigma^- a_k^\dagger + \sigma^+ a_k\right). \tag{2}$$

Its main advantage is the conservation of the number of excitations, making the Hamiltonian solvable.

At resonance $\Delta = \omega_c$, the TLS excited state evolves with the so called Rabi oscillations, which experiment a decay on time due to several sources of energy losses, attributed to either leakage of the cavity or to spurious coupling of the TLS or the cavity to enviromental degrees of freedom. The coupling g/ω_c must be greater than the losses in order to solve these drawbacks, which defines in fact the *strong coupling regime* (SC).

Besides, *ultrastrong coupling regime* (USC) is presented in the context of a larger normalized coupling strength, with $g/\omega_c \cong 0.1$ as a starting point, and thus represents when the coupling strength gets comparable to the bare energies of the system.

Additionally, *deep strong coupling regime* (DSC) appears in when $g/\omega_c > 1$ and higher order perturbative processes become noticeable and even of leading importance.

An important punctualization has to be made. WC, SC, and USC regimes discuss the influence of light-matter coupling strength with respect to different parameters. Whether g/ω_c is weak or strong depends on it being larger or not than the mentioned losses of the system. Complementary to that, USC compares g/ω_c to the bare energies in the system. Consequently, it is possible for a system to be in the USC without having SC if losses are large enough. The scale which defines USC instead regulates whether perturbation theory can be used, as well as the limit where approximations such as the RWA can be applied in light-matter interaction models.

Another aspect to take into account for this work is that the difference between USC and non-USC regimes is specially noteworthy for the ground state (GS) of a coupled light-matter system. For weak couplings the system comprises the atom in its GS inside an empty cavity. With the increasing coupling g/ω_c it becomes more probable to have atomic and photonic virtual excitations in the GS. Then, upon reaching the DSC, the GS of (1) consists of photonic Schrödinger cat states entangled with the atom and exhibits non-classical properties such as squeezing [3].

1.2 Going beyond single mode case

It is true that some of the most paradigmatic models of light-matter interaction like (1) do not neglect some terms which are often ignored at low light-matter coupling strengths g/ω_c. In spite of this, they still depend on some approximations, like the projection of atoms in a two level space (TLS) or the fact of singling out just one mode of light. In recent years some of these approximations have been demonstrated to be unsatisfactory for couplings governing the USC and further regimes. In particular there exists a need to consider multiple modes in the cavity, resulting in significant differences in the dynamics of the system even for apparently non-problematic values of g/ω_c, allowing for superluminal signalling in the DSC regime [4] and thus alerting us that the model becomes unphysical.

Under this backdrop this work will consider an extension of the quantum Rabi model (1) for this multimode case, namely the so-called spin-boson model, given by

$$\mathcal{H}_{SB} = \frac{\Delta}{2}\sigma^x + \sum_k \omega_k b_k^\dagger b_k + \sigma^z \sum_k c_k \left(b_k^\dagger + b_k\right). \tag{3}$$

This is created by the addition of sums for all the considered modes in the bosonic and the interaction term, with the corresponding dispersion relation ω_k and coupling constant c_k, whose expressions will be explained later.

Furthermore, a study of multimode cavities consequently leads us to the consideration of a real-space electric field inside the cavity [4], that is,

$$\vec{E}(x) = i\vec{u}_x \sum_k \left(\frac{\hbar\omega_k}{2\epsilon_0 LA}\right)^{1/2} a_k e^{i(kx-\omega_k t)} + \text{h.c.} \tag{4}$$

Notice that a single relevant polarization along the x axis has been taken into account. Here A is the transverse area of the cavity, L its length, and ϵ_0 is the vacuum permittivity. Besides, periodic boundary conditions have been assumed for simplicity, without loss of generality.

In this Undergraduate Dissertation we have studied the GS properties of the multimode version of the quantum Rabi model (1), that is, the spin-boson model described by (3), throughout the USC and DSC coupling regimes. It has been shown to significantly deviate from the single-mode prediction, confirming the necessity to implement this multimode description.

We have to take into account that the spin-boson Hamiltonian does not have a know solution [6, Chap. 18.1]. Moreover, modern implementations of these models involve high values of the coupling constant g/ω_c, not allowing to apply the usual approximations such as RWA in order to arrive at a solvable Hamiltonian and also making the system more difficult to simulate. Within this context, different numerical techniques have been used to approach this problem, like Matrix Product State (MPS) or Density Matrix Renormalization Group (DMRG), as well as semianalytical treatments as the variational and standard polaron transforms, the former of which is based on a variational *ansatz*. The polaron transform is precisely the tool with which we are going to treat our system, as well as propose a generalized version of it in order to make improvements on its performance.

We expect this study to serve as a review of previous treatments of the polaron transformation and to contribute in more sophisticated implementations of this approach.

1.3 Microscopic derivation of the Rabi model in circuit QED

Although the USC regime has been reached in several solid-state systems recently, the experimental effort required to achieve this regime is still considerable. Furthermore, it remains difficult to probe many interesting system properties in these experiments, especially dynamics, for a wide range of parameters. A suitable platform that allows us to implement this type of systems is the use of superconducting quantum circuits (SQCs) [7, Chap. 4], where properties like resonance frequencies or coupling strength can be designed and even tuned while operating in the microwave (GHz) range and cooled to millikelvin temperatures. That has been exploited in the SC regime, and more remarkably it was the first platform to demonstrate USC and DSC. The main advantage with respect to other experimental systems is that they do not require collective excitations to reach USC.

Entering now in our case, the SQC version of cavity QED is called circuit QED, its representation can be seen in Fig. 2. In order to implement a circuit QED system we firstly cut a transmission line at two ends, for the purpose of converting propagating waves along the line into stationary ones and thus creating a resonator. This implies the mentioned ends will be working as the cavity mirrors for confining photons. Secondly, this is capacitively coupled with "artificial atoms", created from a superconducting qubit (based in Josephson junctions) which can effectively operate as a TLS. In a nutshell, the Josephson junction acts as a non-linear inductor which is paired with a regular capacitor to create an anharmonic oscillator. The increasing spacing of its energy levels makes the two level approximation valid, effectively acting as a qubit when only two levels are addressed. The Hamiltonian of the system reads

$$\mathcal{H} = \hbar\omega \left(a^\dagger a + \frac{1}{2} \right) + \frac{\hbar\omega_{qub}^{CPB}}{2} \sigma^z + \hbar g \left(a^\dagger + a \right) \sigma^x, \tag{5}$$

which matches that of the quantum Rabi Hamiltonian (1). Notice that the equation has been expressed in the single mode case for simplicity, but a similar expression would be obtained for the multimode case given by an spin-boson-like Hamiltonian (3) like the one we are treating on this work.

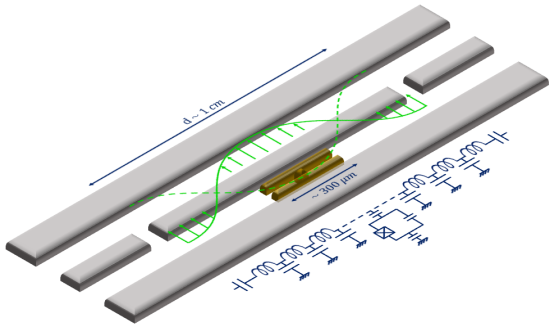

Fig. 2: Schematic representation of a circuit QED system.

2 Ground state calculation

2.1 Variational polaron transform

As we have already mentioned in the previous section, our model comprises a generalized version of the so called variational polaron transform. However, before diving into the generalized one it is interesting to explain a simpler form of itself that has been already used in several works such as [8].

The polaron transform is an analytical technique created for studying a spin-boson-like model beyond the RWA. The low-energy dynamics of the model are comfortably described by first disentangling the TLS and the field with a unitary transformation

$$U_P\left(f_k\right)=\exp\left[-\sigma^z\sum_k\left(f_k b_k^\dagger-f_k^* b_k\right)\right]. \tag{6}$$

It produces a quasi-solvable Hamiltonian in the polaron picture, for which the GS can be calculated with the use of a practical variational *ansatz* given by

$$\left|\Psi_{GS}\left(f_k\right)\right\rangle=U_P\left(f_k\right)\left|S\right\rangle\otimes\left|\vec{0_k}\right\rangle. \tag{7}$$

Where $|S\rangle$ is the spin ground state, easier to deduce in this picture after assuming that the state of the photons is the vacuum, and the f_k are the parameters that can be calculated within the variational method. It yields the transformed spin-boson Hamiltonian

$$\begin{aligned}\mathcal{H}_P=&\frac{\Delta}{2}\exp\left[2\sigma^z\sum_k\left(f_k b_k^\dagger-f_k^* b_k\right)\right]\sigma^x+\sum_k\omega_k b_k^\dagger b_k+\sigma^z\sum_k c_k\left(b_k^\dagger+b_k\right)\\&-\sigma^z\sum_k\omega_k\left(f_k b_k^\dagger+f_k^* b_k\right)+\sum_k\omega_k|f_k|^2-\sum_k c_k\left(f_k+f_k^*\right).\end{aligned} \tag{8}$$

We choose $|S\rangle=|0\rangle$ for the spin state corresponding to the GS (Explanation in A.1). We apply the variational method to determine the expression of the f_k's, minimizing the mean GS energy

$$E_{GS}=\min_{S,f_k}\left\langle\Psi_{GS}\left(f_k\right)\right|\mathcal{H}\left|\Psi_{GS}\left(f_k\right)\right\rangle=-\frac{\Delta_r}{2}+\sum_k\omega_k|f_k|^2-\sum_k c_k\left(f_k+f_k^*\right). \tag{9}$$

Taking real variational parameters, $f_k=f_k^*$, and differentiating with respect to them, we have

$$0=\frac{dE_{GS}}{df_k}=2\Delta_r f_k+2\omega_k f_k-2c_k\Longleftrightarrow f_k=\frac{c_k}{\Delta_r+\omega_k}. \tag{10}$$

With this we have the GS (7) completely defined and we could start the study of its observables and properties in this state. But the main focus of our study will be set on a generalized version of polaron transform. Before moving on, it is important to introduce a non-variational, i.e. a fixed, polaron transform that can also be used to define a ground state *ansatz*. It corresponds to setting $f_k=c_k/\omega_k$ in the derivation above. In fact, the polaron transform was originally formulated this way [5]. It is also important to emphasize at this point that the different *ansätze* that we will be considered are not legitimized *a priori* but *a posteriori*, depending on

how low of an energy they predict for the ground state. This is just to say that the constitute educated guesses for a candidate ground state, and the one that yields the lowest GS energy is chosen as the best.

Our purpose now is move beyond this last calculations, trying to obtain the equivalent expression of the GS from the transformed Hamiltonian in the polaron picture, but this time studying a modified spin-boson Hamiltonian, as a new form of the one given by (3). Specifically, we will introduce a small bias ϵ as a symmetry breaking term in the TLS in order to reach a generalization of the model. Our new biased spin-boson Hamiltonian is given by

$$\mathcal{H}_{BSB} = \frac{\Delta}{2}\sigma^x + \frac{\epsilon}{2}\sigma^z + \sum_k \omega_k b_k^\dagger b_k + \sigma^z \sum_k c_k (b_k^\dagger + b_k). \tag{11}$$

Notice that if the bias ϵ vanishes the problem could be solved with the previously explained variational polaron transform (6). However, in our case an improvement could be the use of an asymmetric *ansatz* [9, 10] such that

$$U_P(f_k, l_k) = \exp\left[\sigma^z \sum_k \left(f_k b_k^\dagger - f_k^* b_k\right) + \sum_k \left(l_k b_k^\dagger - l_k^* b_k\right)\right] = \exp\left[\sigma^z \hat{\alpha} + \hat{\beta}\right]. \tag{12}$$

Here we have defined $\hat{\alpha} = \sum_k \left(f_k b_k^\dagger - f_k^* b_k\right)$ and $\hat{\beta} = \sum_k \left(l_k b_k^\dagger - l_k^* b_k\right)$. Now we have to deduce two variational parameters f_k, l_k instead of one, in order to solve our new *ansatz* for the GS

$$|\Psi_{GS}(f_k, l_k)\rangle = U_P(f_k, l_k)\,|S\rangle \otimes |\vec{0_k}\rangle\,. \tag{13}$$

We will require the Baker-Campbell-Hausdorf (BCH) formula,

$$e^{t(\hat{X}+\hat{Y})} = e^{t\hat{X}} e^{t\hat{Y}} e^{-\frac{t^2}{2}[\hat{X},\hat{Y}]}, \tag{14}$$

provided that the commutator $[\hat{X}, \hat{Y}]$ gives a complex number. The contrary would imply to have an infinite number of nested commutators. In our case $[\hat{\alpha}, \hat{\beta}] = \sum_k (f_k l_k^* - f_k^* l_k) \in \mathcal{C}$ so we can use our form of (14). Afterwards, the variational parameters are taken to be real $f_k, l_k \in \mathbb{R}$, so that $[\hat{\alpha}, \hat{\beta}] = 0$ and thus we can split our generalised polaron transform U_P into two terms

$$U_P(f_k, l_k) = e^{\sigma^z \hat{\alpha}} e^{\hat{\beta}} = U_Z U_{\mathbb{1}}, \tag{15}$$

where we have called for simplicity $U_Z(f_k) = e^{\sigma^z \hat{\alpha}}$ and $U_{\mathbb{1}}(l_k) = e^{\hat{\beta}}$.

Now, apart from general commutator properties, we will be able to transform the Hamiltonian into the polaron picture using (see Appendix A.2 for the demostration)

$$[b_k, U_Z] = \pm \sigma^z f_k U_Z, \tag{16}$$

$$[b_k, U_{\mathbb{1}}] = \pm l_k U_{\mathbb{1}}. \tag{17}$$

By means of these expressions we can extract two useful results that will be extensively used:

$$U_Z^\dagger b_k U_Z = U_Z^\dagger [b_k, U_Z] + (U_Z^\dagger U_Z) b_k = U_Z^\dagger [b_k, U_Z] + b_k = U_Z^\dagger (\sigma^z f_k U_Z) + b_k = \sigma^z f_k + b_k, \tag{18}$$

$$U_{\mathbb{1}}^\dagger b_k U_{\mathbb{1}} = U_{\mathbb{1}}^\dagger [b_k, U_{\mathbb{1}}] + (U_{\mathbb{1}}^\dagger U_{\mathbb{1}}) b_k = U_{\mathbb{1}}^\dagger [b_k, U_{\mathbb{1}}] + b_k = U_{\mathbb{1}}^\dagger (l_k U_{\mathbb{1}}) + b_k = l_k + b_k. \tag{19}$$

Notice that we obtain exactly the same expression when replacing the annihilation operator b_k for the creation one $b_k^\dagger$.

Once all the useful tools for computing the transformed Hamiltonian are at our disposal, we compute it by parts

$$U_P^\dagger \mathcal{H} U_P = U_P^\dagger \mathcal{H}_I U_P + U_P^\dagger \mathcal{H}_M U_P + U_P^\dagger \mathcal{H}_{TLS} U_P. \tag{20}$$

Starting with the interaction term, H_I, it leaves

$$\begin{aligned}
U_P^\dagger \mathcal{H}_I U_P &= U_P^\dagger \left(\sigma^z \sum_k c_k \left(b_k^\dagger + b_k \right) \right) U_P \\
&= U_{\mathbb{1}}^\dagger U_Z^\dagger \left(\sigma^z \sum_k c_k \left(b_k^\dagger + b_k \right) \right) U_Z U_{\mathbb{1}} \\
&= \sigma^z \sum_k c_k \left[\left(U_{\mathbb{1}}^\dagger U_Z^\dagger b_k^\dagger U_Z U_{\mathbb{1}} \right) + \left(U_{\mathbb{1}}^\dagger U_Z^\dagger b_k U_Z U_{\mathbb{1}} \right) \right] \\
&\overset{(18)}{=} \sigma^z \sum_k c_k \left[\left(U_{\mathbb{1}}^\dagger \left(\sigma^z f_k + b_k^\dagger \right) U_{\mathbb{1}} \right) + \left(U_{\mathbb{1}}^\dagger \left(\sigma^z f_k + b_k \right) U_{\mathbb{1}} \right) \right] \\
&\overset{(19)}{=} \sigma^z \sum_k c_k \left[\left(\sigma^z f_k + l_k + b_k^\dagger \right) + \left(\sigma^z f_k + l_k + b_k \right) \right] \\
&= \mathcal{H}_I + 2 \left(\sum_k c_k f_k + \sigma^z \sum_k c_k l_k \right).
\end{aligned} \tag{21}$$

Then we can proceed similarly with the multimode term, $\mathcal{H}_M$, giving

$$\begin{aligned}
U_P^\dagger \mathcal{H}_M U_P &= U_P^\dagger \left(\sum_k \omega_k b_k^\dagger b_k \right) U_P \\
&= \sum_k \omega_k \left[\left(U_P^\dagger b_k^\dagger U_P \right) \left(U_P^\dagger b_k U_P \right) \right] \\
&= \sum_k \omega_k \left[\left(U_{\mathbb{1}}^\dagger U_Z^\dagger b_k^\dagger U_Z U_{\mathbb{1}} \right) \left(U_{\mathbb{1}}^\dagger U_Z^\dagger b_k U_Z U_{\mathbb{1}} \right) \right] \\
&\overset{(18),(19)}{=} \sum_k \omega_k \left[\left(\sigma^z f_k + l_k + b_k^\dagger \right) \left(\sigma^z f_k + l_k + b_k \right) \right] \\
&= \mathcal{H}_M + \sum_k \omega_k \left(f_k^2 + l_k^2 \right) + 2\sigma^z \sum_k \omega_k f_k l_k \\
&+ \sigma^z \sum_k \omega_k f_k \left(b_k^\dagger + b_k \right) + \sum_k \omega_k l_k \left(b_k^\dagger + b_k \right).
\end{aligned} \tag{22}$$

However, for the part regarding the TLS and the bias, H_{TLS}, we will need a different approach, as U_P commutes with σ^z but not with σ^x. We will solve the two different terms separately,

$$U_P^\dagger \mathcal{H}_{TLS} U_P = U_P^\dagger \left(\frac{\Delta}{2}\sigma^x + \frac{\epsilon}{2}\sigma^z \right) U_P = \underbrace{\left[U_{\mathbb{1}}^\dagger U_Z^\dagger \left(\frac{\Delta}{2}\sigma^x \right) U_Z U_{\mathbb{1}} \right]}_{(I)} + \underbrace{\left[U_{\mathbb{1}}^\dagger U_Z^\dagger \left(\frac{\epsilon}{2}\sigma^z \right) U_Z U_{\mathbb{1}} \right]}_{(II)}. \tag{23}$$

Firstly we transform the bias part, which is solved without any problem, doing

$$(II) \to \left[U_{\mathbb{1}}^{\dagger} U_Z^{\dagger} \left(\frac{\epsilon}{2}\sigma^z\right) U_Z U_{\mathbb{1}}\right] = U_{\mathbb{1}}^{\dagger}\left[\frac{\epsilon}{2}\left(U_Z^{\dagger}\left[\sigma^z, U_Z\right] + U_Z^{\dagger} U_Z \sigma^z\right)\right] U_{\mathbb{1}} = \frac{\epsilon}{2}\left(U_{\mathbb{1}}^{\dagger}\sigma^z U_{\mathbb{1}}\right)$$
$$= \frac{\epsilon}{2}\left(U_{\mathbb{1}}^{\dagger}\left[\sigma^z, U_{\mathbb{1}}\right] + U_{\mathbb{1}}^{\dagger} U_{\mathbb{1}}\sigma^z\right) = \frac{\epsilon}{2}\sigma^z. \tag{24}$$

For the other part we will manage expressions with different Pauli matrices, so it is convenient to use a series expansion to handily express U_Z and $U_Z^{\dagger}$ as combinations of σ^z and $\mathbb{1}$, that is,

$$U_Z = e^{\sigma^z \hat{\alpha}} = \sum_n \frac{(\sigma^z \hat{\alpha})^n}{n!} = \sum_n \frac{\hat{\alpha}^{2n}}{(2n)!} + \sigma^z \sum_n \frac{\hat{\alpha}^{2n+1}}{(2n+1)!} = \cosh\hat{\alpha} + \sigma^z \sinh\hat{\alpha}, \tag{25}$$

$$U_Z^{\dagger} = e^{-\sigma^z \hat{\alpha}} = \sum_n \frac{(-1)^n (\sigma^z \hat{\alpha})^n}{n!} = \sum_n \frac{\hat{\alpha}^{2n}}{(2n)!} - \sigma^z \sum_n \frac{\hat{\alpha}^{2n+1}}{(2n+1)!} = \cosh\hat{\alpha} - \sigma^z \sinh\hat{\alpha}. \tag{26}$$

Now we can compute

$$\begin{aligned} U_Z^{\dagger}\sigma^x U_Z &= (\cosh\hat{\alpha} - \sigma^z \sinh\hat{\alpha})\sigma^x(\cosh\hat{\alpha} + \sigma^z \sinh\hat{\alpha}) \\ &= \sigma^x \cosh^2\hat{\alpha} + \sigma^x\sigma^z \cosh\hat{\alpha}\sinh\hat{\alpha} - \sigma^z\sigma^x \sinh\hat{\alpha}\cosh\hat{\alpha} - \sigma^z\sigma^x\sigma^z \sinh^2\hat{\alpha} \\ &= \sigma^x \cosh^2\hat{\alpha} + \sigma^x \sinh^2\hat{\alpha} - 2\sigma^z\sigma^x \cosh\hat{\alpha}\sinh\hat{\alpha} \\ &= (\cosh(2\hat{\alpha}) - \sigma^z \sinh(2\hat{\alpha}))\sigma^x \\ &= e^{-\sigma^z 2\hat{\alpha}}\sigma^x. \end{aligned} \tag{27}$$

And finally leaving

$$(I) \to \left[U_{\mathbb{1}}^{\dagger} U_Z^{\dagger}\left(\frac{\Delta}{2}\sigma^x\right) U_Z U_{\mathbb{1}}\right] = \frac{\Delta}{2} U_{\mathbb{1}}^{\dagger}\left(e^{-\sigma^z 2\hat{\alpha}}\sigma^x\right) U_{\mathbb{1}} = \frac{\Delta}{2} e^{-\sigma^z 2\hat{\alpha}}\sigma^x$$
$$= \frac{\Delta}{2}\exp\left[-2\sigma^z \sum_k f_k\left(b_k^{\dagger} - b_k\right)\right]\sigma^x. \tag{28}$$

Joining both parts we obtain

$$U_P^{\dagger} H_{TLS} U_P = \frac{\Delta}{2}\exp\left[-2\sigma^z \sum_k f_k\left(b_k^{\dagger} - b_k\right)\right]\sigma^x + \frac{\epsilon}{2}\sigma^z. \tag{29}$$

Now it is interesting to transform the exponential in order to have something more comfortable to diagonalize later. We start applying BCH formula (14), so that

$$\begin{aligned} U_P^{+} H_{TLS} U_P = \frac{\Delta}{2}\exp\left\{-\frac{1}{2}\left[-2\sigma^z \sum_k f_k b_k^{\dagger}, +2\sigma^z \sum_k f_k b_k\right]\right\}\cdot \\ \cdot \exp\left[-2\sigma^z \sum_k f_k b_k^{\dagger}\right]\cdot \exp\left[+2\sigma^z \sum_k f_k b_k\right]\sigma^x + \frac{\epsilon}{2}\sigma^z \\ = \frac{\Delta_r}{2}\cdot \exp\left[-2\sigma^z \sum_k f_k b_k^{\dagger}\right]\cdot \exp\left[+2\sigma^z \sum_k f_k b_k\right]\sigma^x + \frac{\epsilon}{2}\sigma^z, \end{aligned} \tag{30}$$

where the qubit or tunneling frequency has been renormalized to

$$\Delta_r = \Delta e^{-2\sum_k |f_k|^2}. \tag{31}$$

We can apply the same procedure we have used in (25) and (26) with the remaining exponentials, now giving

$$\exp\left[-2\sigma^z\sum_k f_k b_k^\dagger\right] = \sum_n \frac{\left(2\sum_k f_k b_k^\dagger\right)^n (-1)^n (\sigma^z)^n}{n!} = \sum_n \frac{\left(2\hat{\xi}\right)^n (-1)^n (\sigma^z)^n}{n!}$$
$$= \sum_n \frac{\left(2\hat{\xi}\right)^{2n}}{(2n)!} - \sigma^z \sum_n \frac{\left(2\hat{\xi}\right)^{2n+1}}{(2n+1)!} = \cosh 2\hat{\xi} - \sigma^z \sinh 2\hat{\xi}, \tag{32}$$

$$\exp\left[+2\sigma^z\sum_k f_k b_k\right] = \sum_n \frac{(2\sum_k f_k b_k)^n (\sigma^z)^n}{n!} = \sum_n \frac{(2\hat{\gamma})^n (\sigma^z)^n}{n!}$$
$$= \sum_n \frac{(2\hat{\gamma})^{2n}}{(2n)!} + \sigma^z \sum_n \frac{(2\hat{\gamma})^{2n+1}}{(2n+1)!} = \cosh 2\hat{\gamma} + \sigma^z \sinh 2\hat{\gamma}. \tag{33}$$

Here we have defined $\hat{\xi} = \sum_k f_k b_k^\dagger$ and $\hat{\gamma} = \sum_k f_k b_k$. Now we should do the product of (32) and (33), obtaining

$$\begin{aligned}
&\exp\left[-2\sigma^z\sum_k f_k b_k^\dagger\right] \cdot \exp\left[+2\sigma^z\sum_k f_k b_k\right] \\
&= \left(\cosh\hat{\xi} - \sigma^z\sinh\hat{\xi}\right)(\cosh\hat{\gamma} + \sigma^z\sinh\hat{\gamma}) \\
&= \cosh\hat{\xi}\cosh\hat{\gamma} - \sinh\hat{\xi}\sinh\hat{\gamma} + \sigma^z\cosh\hat{\xi}\sinh\hat{\gamma} - \sigma^z\sinh\hat{\xi}\cosh\hat{\gamma} \\
&= \cosh\left(\hat{\xi}-\hat{\gamma}\right) - \sigma^z\sinh\left(\hat{\xi}-\hat{\gamma}\right) \\
&= \cosh(2\hat{\alpha}) - \sigma^z\sinh(2\hat{\alpha}).
\end{aligned} \tag{34}$$

At the end we get

$$U_P^\dagger \mathcal{H}_{TLS} U_P = \frac{\Delta_r}{2}\sigma^x\cosh(2\hat{\alpha}) - \frac{\Delta_r}{2}\sigma^z\sigma^x\sinh(2\hat{\alpha}) + \frac{\epsilon}{2}\sigma^z. \tag{35}$$

We have already calculated every term of the transformed Hamiltonian, which has the form

$$\begin{aligned}
\mathcal{H}_P &= (\mathcal{H}_I)_P + (\mathcal{H}_B)_P + (\mathcal{H}_{TLS})_P = \sigma^z\sum_k c_k\left(b_k^\dagger + b_k\right) + 2\left(\sum_k c_k f_k + \sigma^z\sum_k c_k l_k\right) \\
&+ \sum_k \omega_k b_k^\dagger b_k + \sum_k \omega_k\left(f_k^2 + l_k^2\right) + 2\sigma^z\sum_k \omega_k f_k l_k + \sigma^z\sum_k \omega_k f_k\left(b_k^\dagger + b_k\right) \\
&+ \sum_k \omega_k l_k\left(b_k^\dagger + b_k\right) + \frac{\Delta_r}{2}\sigma^x\cosh(2\hat{\alpha}) - \frac{\Delta_r}{2}\sigma^z\sigma^x\sinh(2\hat{\alpha}) + \frac{\epsilon}{2}\sigma^z \\
&= \frac{\Delta_r}{2}\sigma^x + \frac{\epsilon_r}{2}\sigma^z + \sum_k \omega_k b_k^+ b_k + \sum_k \omega_k l_k\left(b_k^\dagger + b_k\right) - \Delta_r\sigma^z\sigma^x\sum_k f_k\left(b_k^\dagger - b_k\right) \\
&+ \sigma^z\sum_k (c_k + \omega_k f_k)\left(b_k^\dagger + b_k\right) + 2\sum_k c_k f_k + \sum_k \omega_k\left(f_k^2 + l_k^2\right).
\end{aligned} \tag{36}$$

We have expanded the hyperbolic sine and cosine to the 1st order, as well as defined the renormalized the bias as

$$\epsilon_r = \epsilon + 4\sum_k c_k l_k + 4\sum_k \omega_k f_k l_k. \tag{37}$$

2.2 TLS diagonalization

Looking at our new transformed Hamiltonian (36), we will focus on what we can call for simplicity the transformed TLS part, that is,

$$(\mathcal{H}_{TLS})_P = \frac{\Delta_r}{2}\sigma^x + \frac{\epsilon_r}{2}\sigma^z = \frac{1}{2}\begin{pmatrix} \Delta_r & \epsilon_r \\ \epsilon_r & -\Delta_r \end{pmatrix}, \tag{38}$$

proceeding to diagonalize it in order to have a more manageable expression. Notice that the matrix representation has been given in the basis of eigenvectors of σ^x, where we will remain for the following calculations. The eigenvalues of this matrix are

$$\pm W_r = \pm\sqrt{\Delta_r^2 + \epsilon_r^2}. \tag{39}$$

Now we can choose the following eigenvectors for the new "TLS basis" as

$$|-W_r\rangle = \left(\sin\left(\frac{\theta}{2}\right), -\cos\left(\frac{\theta}{2}\right)\right)^T, \tag{40}$$

$$|W_r\rangle = \left(\cos\left(\frac{\theta}{2}\right), \sin\left(\frac{\theta}{2}\right)\right)^T. \tag{41}$$

Here $\cos\theta = \frac{\Delta_r}{W_r}$, $\sin\theta = \frac{\epsilon_r}{W_r}$. In order to have $(0,1)^T$ as the Ground State, we set $|-W_r\rangle$ the second eigenvector. Consequently (38) can be written diagonal is this basis, leaving

$$(\mathcal{H}_{TLS})_P = \frac{1}{2}\begin{pmatrix} W_r & 0 \\ 0 & -W_r \end{pmatrix}. \tag{42}$$

And thus the basis change matrix is

$$A = \begin{pmatrix} \cos\left(\frac{\theta}{2}\right) & -\sin\left(\frac{\theta}{2}\right) \\ \sin\left(\frac{\theta}{2}\right) & \cos\left(\frac{\theta}{2}\right), \end{pmatrix} \tag{43}$$

so that the TLS operators change as

$$A^\dagger\sigma^x A = \cos\theta\sigma^x - \sin\theta\sigma^z, \tag{44}$$

$$A^\dagger\sigma^z A = \cos\theta\sigma^z + \sin\theta\sigma^x. \tag{45}$$

Now we are able to express the transformed Hamiltonian in the new basis, applying the changes given by (45) and (44), resulting in

$$\begin{aligned}\mathcal{H}_P = \frac{W_r}{2}\sigma^x + \sum_k \omega_k b_k^\dagger b_k + \sum_k \omega_k l_k\left(b_k^\dagger + b_k\right) - \Delta_r\sigma^z\sigma^x\sum_k f_k\left(b_k^\dagger - b_k\right) \\ + \left(\cos\theta\sigma^z + \sin\theta\sigma^x\right)\sum_k\left(c_k + \omega_k f_k\right)\left(b_k^\dagger + b_k\right) + 2\sum_k c_k f_k + \sum_k \omega_k\left(f_k^2 + l_k^2\right).\end{aligned} \tag{46}$$

Finally, with our transformed Hamiltonian, we can compute the GS energy using the *ansatz* (13), obtaining

$$\begin{aligned}E_{GS} &= \min_{S,f_k,l_k}\langle\Psi_{GS}(f_k,l_k)|\,\mathcal{H}\,|\Psi_{GS}(f_k,l_k)\rangle = \langle\hat{0}_k|\langle S|\,\mathcal{H}_P\,|S\rangle\,|\hat{0}_k\rangle \\ &= -\frac{W_r}{2} + 2\sum_k c_k f_k + \sum_k \omega_k\left(f_k^2 + l_k^2\right).\end{aligned} \tag{47}$$

2.3 Obtention of variational parameters f_k, l_k for different coupling strenghts

In the original polaron case we applied the variational method in order to determine the variational parameters by minimizing the energy, but here we will choose f_k and l_k conveniently so that the Hamiltonian preserves the number of excitations. In order to do so, we match terms in (46) to obtain a convenient expression of $\mathcal{H}_P$. We compute two different forms of parameterization obtaining two possible effective Hamiltonians for further discussion of the best option between them.

First, by manipulating and rearranging the terms in (46) we obtain f_k and l_k (demonstration given in Appendix A.3),

$$f_k = -\frac{c_k}{W_r + \omega_k}, \tag{48}$$

$$l_k = \frac{c_k}{\omega_k}\frac{\epsilon_r}{W_r + \omega_k}, \tag{49}$$

leaving an effective Hamiltonian

$$\begin{aligned}(\mathcal{H}_{\text{eff},1})_P = \frac{W_r}{2}\sigma^x + \sum_k \omega_k b_k^\dagger b_k + (\sigma^z + \mathbb{1})\sum_k \omega_k l_k \left(b_k^\dagger + b_k\right) \\ - 2\Delta_r \sum_k f_k \left(\sigma^- b_k^\dagger + \sigma^+ b_k\right) + 2\sum_k c_k f_k + \sum_k \omega_k \left(f_k^2 + l_k^2\right).\end{aligned} \tag{50}$$

Notice that the expression of the renormalized bias ϵ_r (37) has changed due to (48) and (49):

$$\epsilon_r = \epsilon + 4\sum_k c_k l_k + 4\sum_k \omega_k f_k l_k = \epsilon + 4\sum_k \frac{c_k^2}{\omega_k}\frac{\epsilon_r W_r}{(W_r + \omega_k)^2} = \epsilon + 4\sum_k \frac{c_k l_k W_r}{(W_r + \omega_k)} \tag{51}$$

Secondly, we can opt for a fixed Polaron transform, as introduced earlier, which yields (procedure shown as well in A.3)

$$(\mathcal{H}_{\text{eff},2})_P = \frac{W_r}{2}\sigma^x + \sum_k \omega_k b_k^\dagger b_k - \Delta_r \sigma^z \sigma^x \sum_k f_k \left(b_k^\dagger - b_k\right) + 2\sum_k c_k f_k + \sum_k \omega_k f_k^2, \tag{52}$$

Which amounts to fixing the variational parameters to

$$f_k = -\frac{c_k}{\omega_k}, \tag{53}$$

$$l_k = 0. \tag{54}$$

The act of fixing $l_k = 0$ in our improved polaron transform (12) implies recovering the original one given by (6) [5], and consequently our comparation between both parameterizations will determine whether our proposed new *ansatz* is better or not than the previously used one.

Finally we have our expressions for the variational parameters f_k and l_k in both parameterizations, with which our GS *ansatz* given by (13) is fully determined. Thanks to it in the next section we will be able to study some properties and observables like the GS energy we have just obtained in previous calculations.

3 Results and analysis

For the whole section our study will focus in the range of resonance and the energy scale will be normalized by ω_c so that $\omega_c = \Delta = 1$. Besides, our range for the normalized coupling strength g/ω_c will cover not only the USC but also the DSC regime. It has to be taken into account that the frequency of the different modes will correspond to $\omega_k = k\omega_c \ \forall k = 1, ..., M$ and the coupling constants will depend on the number of modes k

$$c_k = g \sin\left(\frac{k\pi x_0}{L}\right) \frac{\sqrt{k}}{1 + \delta\,(k-1)} = g \sin\left(k\frac{\pi}{2}\right) \frac{\sqrt{k}}{1 + \delta\,(k-1)}, \tag{55}$$

where δ works as a cutoff in order to avoid the latter equation to diverge [11], where L is the length of the cavity and x_0 is the position of the TLS inside the cavity. For simplicity, $L = 1$ and we place the atom in the centre of the cavity, that is, $x_0 = 1/2$. Furthermore, the considered bias $\epsilon = 0.001$ will remain small and constant in the whole work.

We have two effective forms of $\mathcal{H}_P$ (36) depending on the different expressions of the variational parameters f_k, l_k we have obtained, those given by (48) and (49), and the ones given by (53) and (54). We will now determine the best between our two polaron parameterizations via GS energy comparison, followed by the study of the renormalized parameters and several observables in the GS of the system within our chosen parameterization. Afterwards we will validate our model with the exact diagonalisation of the Hamiltonian $\mathcal{H}_{BSB}$ (11), and we will finish analyzing the profile of electric field inside our cavity. In general, we will carry a comprehensive study of the model across the different regimes of normalized coupling g/ω_c as well as the different number of modes M. This includes a comparison with the standard single-mode case.

3.1 Choice of the best parameterization

Our initial purpose will be to discern which parameterization yields a lower energy for the candidate GS, indicating that it is the superior ansatz, and thus will be selected for studying the observables of our model.

In order to do that, we compare the GS energy given by (47) for both parameterizations in Fig. 3 seeking the one with the minimal energy. The effect of the increasing number of modes M and normalized coupling strength g/ω_c is a progressive decrease of the energy to decrease in both cases.

Focusing on our purpose, the tendencies of both parameterizations show almost identical values, making it impossible to choose one of them. Because of that, we compute the difference between both energies, that is, $\delta E_{GS} = E_{GS,1} - E_{GS,2}$ in Fig. 4. Here we observe a convergence for $M > 500$. We establish the first parameterization as the best fit for the model due to having the minimal energy regardless of the number of modes, confirming successfully that our improved polaron *ansatz* (13) fits better for studying the model than the original one (7).

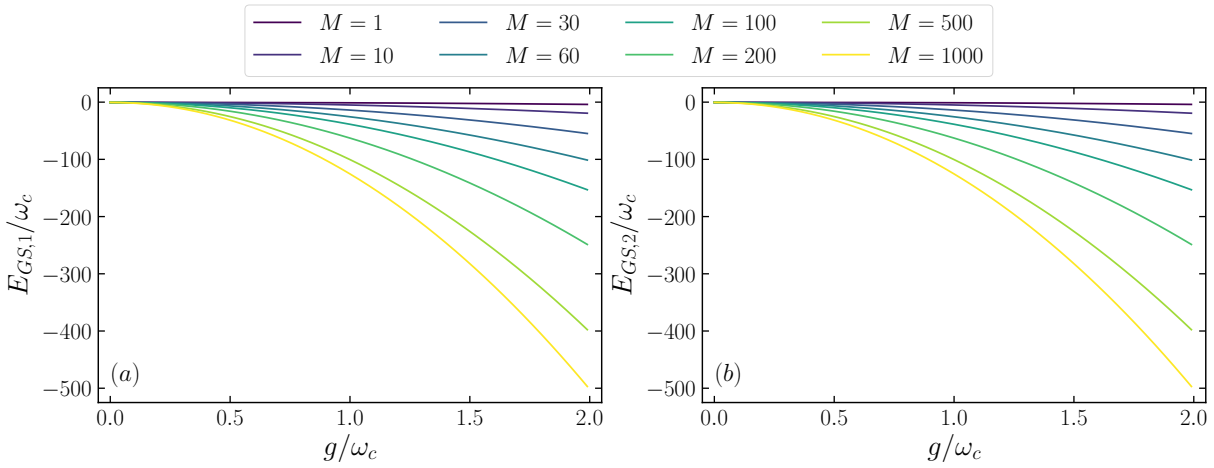

Fig. 3: Ground State energy as a function of the normalized coupling strength g/ω_c and the number of modes M. Computation for the first parameterization at left (a) and for the second parameterization at right (b). Parameters: $\omega_c = 1$, $\Delta = 1$, $\epsilon = 0.001$, $\delta = 0.003$, $L = 1$, $x_0 = 1/2$.

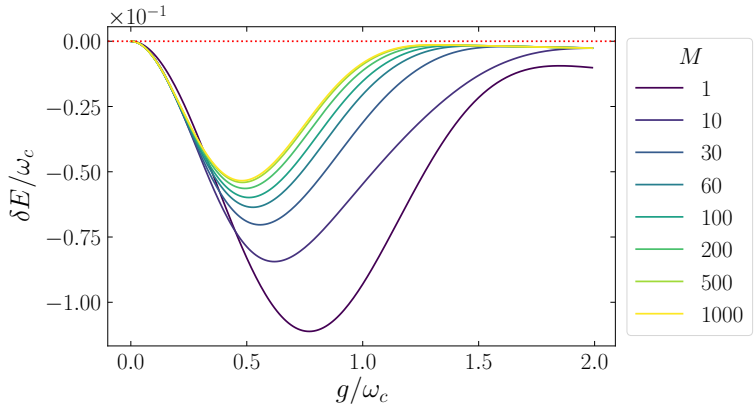

Fig. 4: Energy difference δE_{GS} between the first and second parameterization, as a function of the normalized coupling strength g/ω_c and the number of modes M. Dotted red line in y=0 emphasizes that $E_{GS,1} < E_{GS,2}$, $\forall\ g/\omega_c, M$. Parameters: $\omega_1 = 1$, $\Delta = 1$, $\epsilon = 0.001$, $\delta = 0.003$, $L = 1$, $x_0 = 1/2$.

3.2 Renormalized parameters Δ_r and ϵ_r

As we have seen in the previous section, during the obtention of the transformed Hamiltonian $\mathcal{H}_P$ (36), the qubit or tunneling frequency Δ and the bias ϵ have been renormalized with expressions corresponding with (31) and (37) respectively.

In Fig. 5 we compute the quotient between the renormalized parameters and the bare ones for the chosen parameterization. Focusing on Fig. 5(a), the renormalized qubit frequency Δ_r vanishes or, in other words, the energy gap closes, for a finite value of g/ω_c when approaching the DSC regime. This tendency comes about sooner with an increase of the number of modes M until it converges for $M > 500$ modes. Besides, in Fig. 5(b) is shown the quotient between the renormalized bias, ϵ_r, and the initial one, ϵ. Renormalized bias gets smoothly higher with the coupling until it also converges even sooner than the frequency, as soon as it arrives to $M > 200$

modes approximately.

Moreover, it has to be known that the equations corresponding to the renormalized frequency and bias have been solved iteratively for the chosen parameterization as they are self-consistent equations, i.e. functions of themselves, as can be seen in

$$\Delta_r \overset{(48)}{=} \Delta \exp\left[-2\sum_k \left|-\frac{c_k}{W_r+\omega_k}\right|^2\right] \overset{(39)}{=} \Delta \exp\left[-2\sum_k \left|-\frac{c_k}{\sqrt{\Delta_r^2+\epsilon_r^2}+\omega_k}\right|^2\right], \tag{56}$$

$$\epsilon_r \overset{(51)}{=} \epsilon + 4\sum_k \frac{c_k^2}{\omega_k}\frac{\epsilon_r W_r}{(W_r+\omega_k)^2} \overset{(39)}{=} \epsilon + 4\sum_k \frac{c_k^2}{\omega_k}\frac{\epsilon_r\sqrt{\Delta_r^2+\epsilon_r^2}}{\left(\sqrt{\Delta_r^2+\epsilon_r^2}+\omega_k\right)^2}. \tag{57}$$

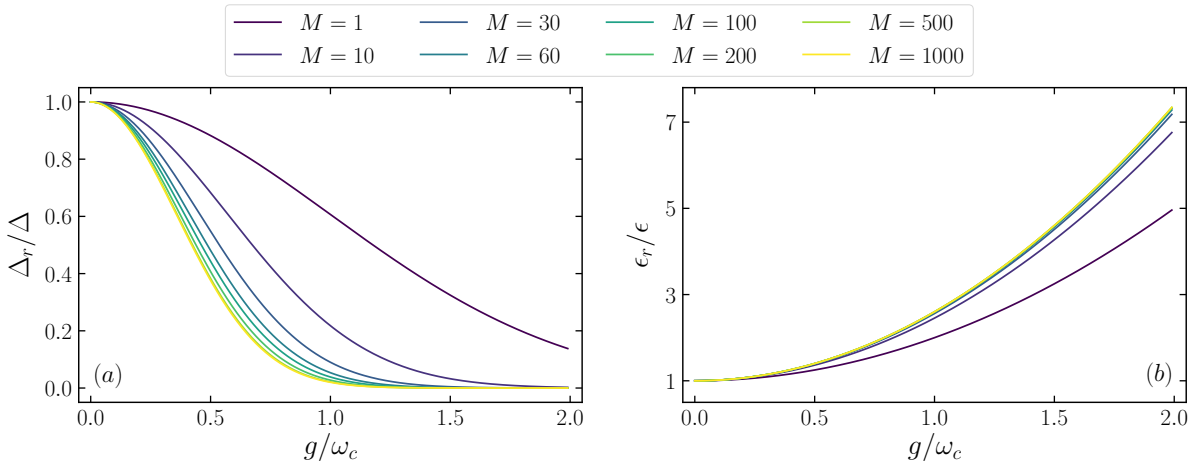

Fig. 5: Renormalised parameters in units of the bare ones for the chosen parameterization, as a function of the normalized coupling strength g/ω_c and the number of modes M. In (a) is depicted Δ_r in units of the bare one Δ, and in (b) is plotted ϵ_r in units of ϵ. Parameters: $\omega_c = 1$, $\Delta = 1$, $\epsilon = 0.001$, $\delta = 0.003$, $L = 1$, $x_0 = 1/2$.

3.3 Computation of ground state observables

Now we can proceed with the study of the GS observables within our chosen parameterization. First of all we will turn the scope to the evolution of the spin in our GS by computing the absolute mean values of σ^x and σ^z in Fig. 6, given by

$$\langle\sigma^x\rangle = \langle\Psi_{GS}(f_k,l_k)|\,\sigma^x\,|\Psi_{GS}(f_k,l_k)\rangle \overset{(28)}{=} \frac{\Delta_r}{\Delta}\langle\vec{0}_k|\langle S|\,\sigma^x\,|S\rangle\,|\vec{0}_k\rangle \overset{(44)}{=} -\frac{\Delta_r^2}{W_r\Delta}, \tag{58}$$

$$\langle\sigma^z\rangle = \langle\Psi_{GS}(f_k,l_k)|\,\sigma^z\,|\Psi_{GS}(f_k,l_k)\rangle \overset{(24)}{=} \langle\vec{0}_k|\langle S|\,\sigma^z\,|S\rangle\,|\vec{0}_k\rangle \overset{(45)}{=} -\frac{\epsilon_r}{W_r}. \tag{59}$$

As we can confirm, the projection of the spin in x, z axes changes while increasing g/ω_c, being at its majority in x at lower values of the normalized coupling strength until it is mostly in z for higher values. The effect of the number of modes in these spin observables is revealed again as a convergence of the curves at $M > 500$ modes, that is, the same behaviour as in Fig. 5(a) with the renormalized qubit frequency Δ_r, observed less clearly for $\langle\sigma^z\rangle$ as it is modulated by the smoothly increasing value of the renormalized bias ϵ_r, as can be remembered from Fig. 5(b).

This effect comes from the expressions of the mean values given by (58) and (59), depending precisely on these renormalized parameters.

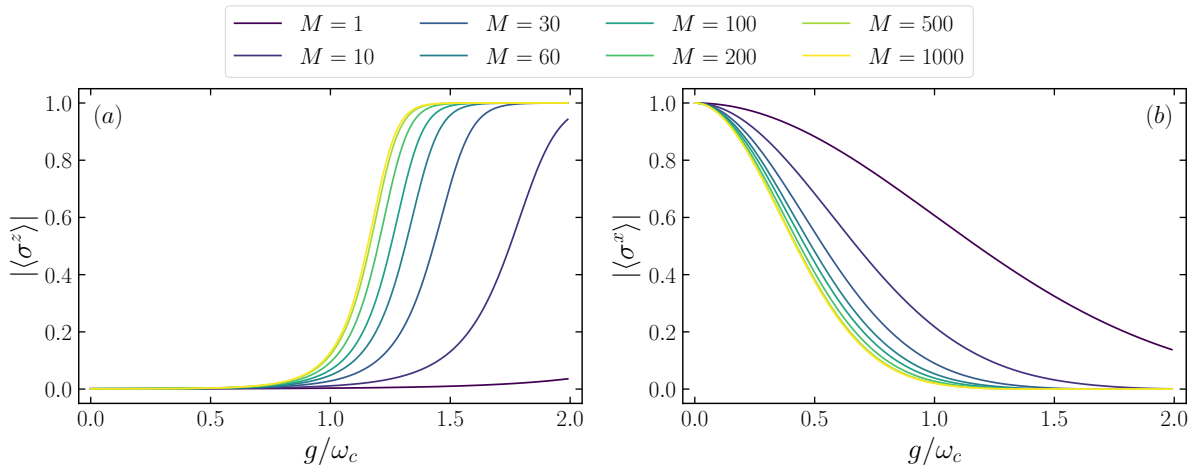

Fig. 6: Absolute value of spin GS observables $\langle\sigma^z\rangle$ and $\langle\sigma^x\rangle$ for the chosen parameterization, as a function of the normalized coupling strength g/ω_c and the number of modes M. Absolute values are plotted in order to make the analysis more comfortable. Parameters: $\omega_c = 1$, $\Delta = 1$, $\epsilon = 0.001$, $\delta = 0.003$, $L = 1$, $x_0 = 1/2$.

We can further characterise the GS by computing another spin observable as is the population of the TLS $P_e = \langle\sigma^+\sigma^-\rangle$, i.e. the GS probability of having an excited spin, as can be seen in Fig. 7. The expression for P_e is

$$\begin{aligned} P_e &= \langle\Psi_{GS}(f_k, l_k)|\,\sigma^+\sigma^-\,|\Psi_{GS}(f_k, l_k)\rangle \\ &= \frac{1 + \langle\Psi_{GS}(f_k, l_k)|\,\sigma^x\,|\Psi_{GS}(f_k, l_k)\rangle}{2} \overset{(59)}{=} \frac{1 - \frac{\Delta_r^2}{W_r\Delta}}{2}. \end{aligned} \tag{60}$$

Notice that here $\sigma^+\sigma^- = \frac{1}{2}(\sigma^x + \mathbb{1})$ has been used. This is a direct consequence of the renormalization of the qubit frequency Δ. It starts at $P_e = 0$, and as soon as g/ω_c increases it remains stable at $P_e = 0.5$ for a sufficiently high coupling, effect that becomes more prominent when M increases and even converges again for $M > 500$ modes.

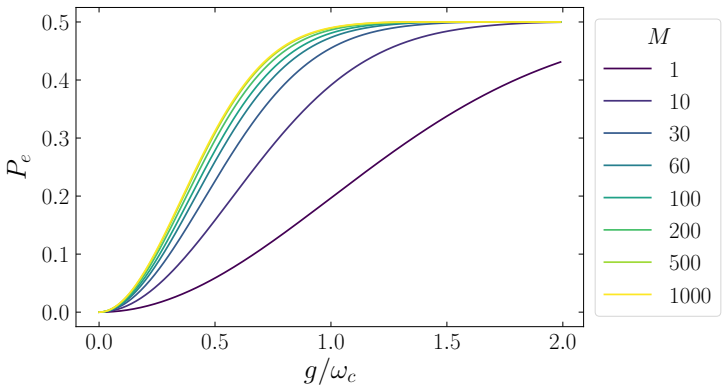

Fig. 7: Probability of having a Ground State with a excited spin P_e, that is, the population of the Ground State, as a function of the normalized coupling strength g/ω_c and the number of modes M. It is a direct consequence of $\langle\sigma^z\rangle$. Parameters: $\omega_c = 1$, $\Delta = 1$, $\epsilon = 0.001$, $\delta = 0.003$, $L = 1$, $x_0 = 1/2$.

3.4 Exact diagonalization of the Hamiltonian and efficiency of the model

We are also interested in making the definitive validation of our parameterization with the improved polaron transform, by comparing it with the exact diagonalization of the model given in (11). The dimension of the Hamiltonian is remarkable, taking into account that it is the Kroenecker product of different Hilbert spaces

$$\mathcal{H}_{BSB} = \mathcal{H}_S \otimes \mathcal{H}_{ph} = \mathcal{H}_S \otimes \mathcal{H}_1 \otimes \cdots \otimes \mathcal{H}_M. \tag{61}$$

A conflict is presented on the need of an infinite state-space in order to have a real exact diagonalization, added to the fact that it grows exponentially with the number of modes M. Therefore, we can discern that the exact diagonalization will be very limited in terms of computational capability. The procedure to follow is to set a cutoff in the dimension of the bosonic state-space, n_{cutoff}, and afterwards to reach a compromise between the number of modes M and n_{cutoff} in order to have as reliable results as possible, with a computationally tractable finite-size Hamiltonian so that

$$\dim(\mathcal{H}_{BSB}) = 2(n_{\text{cutoff}} + 1)^M. \tag{62}$$

On the one hand, we compare the GS energy from our improved polaron with the obtained in the exact diagonalization in Fig. 8. For computing this we smoothly increase the state-space dimension for a fixed number of modes M with the purpose of reaching convergence at some finite value of n_{cutoff}, i.e., that if we continue increasing n_{cutoff} no change in the tendency is observed.

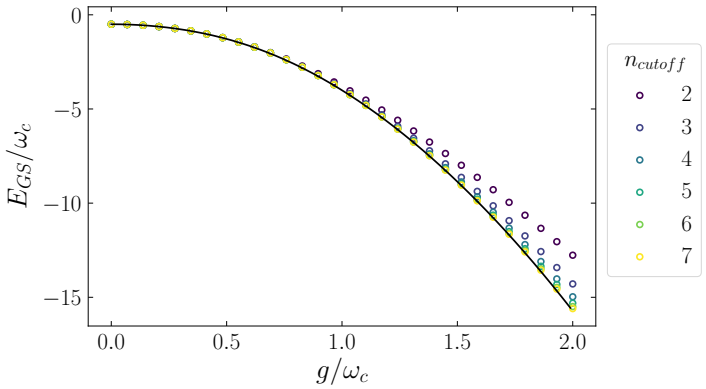

Fig. 8: Ground State energy computed by exact diagonalisation of the Hamiltonian, as a function of the normalized coupling strength g/ω_c and the dimension of the photons space n_{cutoff} for a fixed number of modes $M = 7$. Black line represents the same computation for our improved polaron. Almost perfect agreement between the exact and the polaron plot as soon as n_{cutoff} is slightly increased. Parameters: $M = 7$, $\omega_c = 1$, $\Delta = 1$, $\epsilon = 0.001$, $\delta = 0.003$, $L = 1$, $x_0 = 1/2$.

However, a complete convergence is not reached at the end of our computational capabilities. In spite of that, an agreement is almost satisfactorily obtained with respect to the polaron computation except for our highest values of the normalized coupling strength g/ω_c.

On the other hand, a comparison of the absolute value of spin observables $\langle\sigma^x\rangle$ and $\langle\sigma^z\rangle$ given by (58) and (59) is computed in Fig. 9. This time the strategy is to set a n_{cutoff}, i.e. a constant dimension of the state-space, and smoothly increase the number of modes M until the end of our computational capability, in order to observe the tendency and compare the results with the obtained within our polaron model. If we presume the result given at $M = 1000$ by polaron to be the most accurate value for the mean value of the spin observables we have obtained on this work, besides the fact that our exact diagonalization computation approaches to it by increasing the number of modes M, our conclusion is that the improved *ansatz* would presumably reproduce accurately the values obtained by the exact diagonalization if infinite computational capability were available.

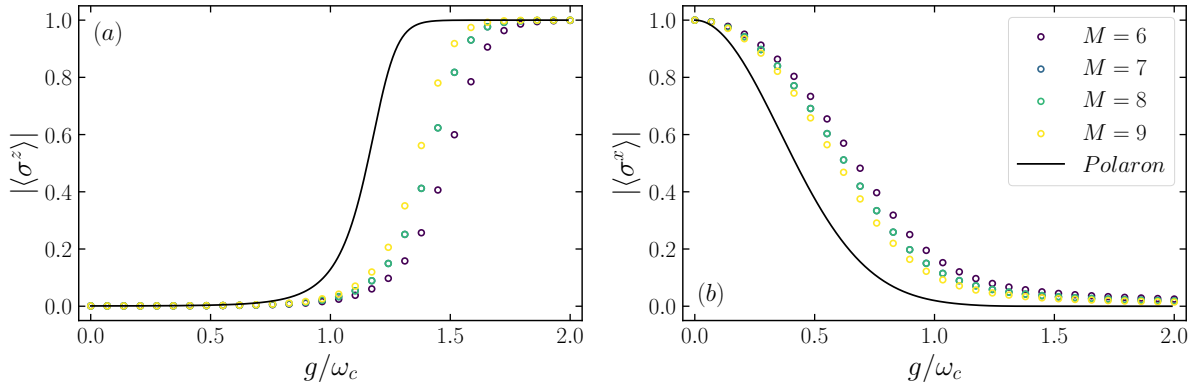

Fig. 9: Spin observables $\langle\sigma^z\rangle$ and $\langle\sigma^x\rangle$ computed by exact diagonalisation of the Hamiltonian, as a function of the normalized coupling strength g/ω_c and the number of modes M for a fixed $n_{\text{cutoff}} = 5$. Black line computes the same computation for our improved polaron at $M = 1000$. Parameters: $n_{\text{cutoff}} = 5$, $\omega_c = 1$, $\Delta = 1$, $\epsilon = 0.001$, $\delta = 0.003$, $L = 1$, $x_0 = 1/2$.

3.5 Electric field inside the cavity

Lastly, it is also interesting to compute the profile of the GS mean electric field inside the cavity (4), which contains the TLS at the centre as we have explained at the beginning of this section, that is,

$$\langle E^+(x)\rangle = \sqrt{\frac{\hbar}{\epsilon_0\nu}}\sum_k \sqrt{\omega_k}\langle b_k\rangle \sin\left(\frac{k\pi x}{L}\right) \overset{L,\hbar,\epsilon_0,\nu=1}{=} \sum_k \frac{c_k\epsilon_r}{\sqrt{\omega_k}W_r}\sin(k\pi x), \tag{63}$$

where c_k is given by (55) and W_r by (39), aside from

$$\begin{aligned}\langle b_k\rangle &\overset{(45)}{=} \langle\Psi_{GS}(f_k,l_k)|\, b_k\, |\Psi_{GS}(f_k,l_k)\rangle \\ &= \langle\vec{0}_k|\langle S|\left[b_k - \frac{c_k}{W_r+\omega_k}\left(\frac{\Delta_r}{W_r}\sigma^x + \frac{\epsilon_r}{W_r}\sigma^z - \frac{\epsilon_r}{\omega_k}\right)\right]|S\rangle\,|\vec{0}_k\rangle = \frac{c_k\epsilon_r}{\omega_k W_r}.\end{aligned} \tag{64}$$

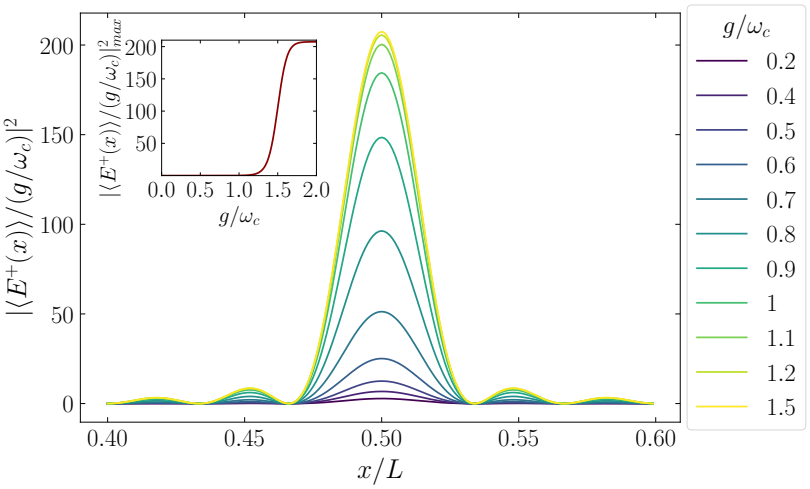

Fig. 10: Spatial Ground State distribution of the electric field inside the cavity (63), as a function of the normalized coupling strength g/ω_c and the position of the TLS inside the cavity. Parameters: $M = 30$, $\omega_c = 1$, $L = 1$, $x_0 = 0.5$, $\delta = 0.003$, $\Delta = 1$, $\epsilon = 0.001$, $L = 1$, $x_0 = 1/2$. Inset corresponding to the maximum values of the distribution as a function of the normalized coupling strength g/ω_c.

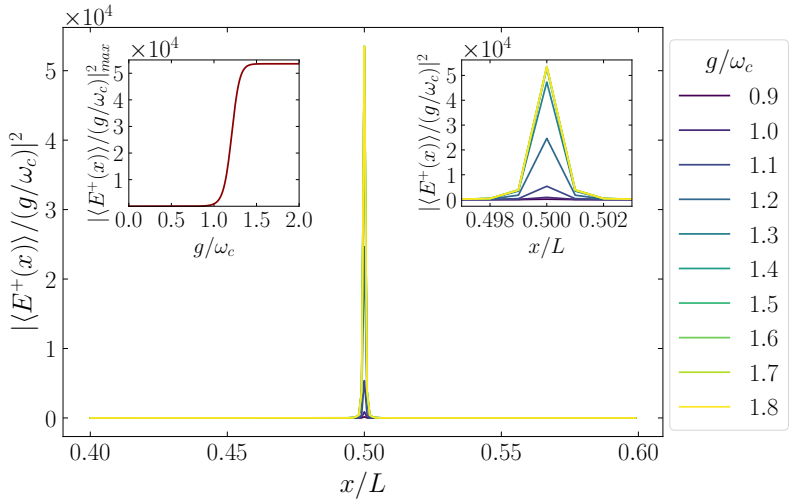

Fig. 11: Spatial Ground State distribution of the electric field inside the cavity, as a function of the normalized coupling strength g/ω_c and the position of the TLS inside the cavity. Parameters: $M = 1000$, $\omega_c = 1$, $L = 1$, $x_0 = 0.5$, $\delta = 0.003$, $\Delta = 1$, $\epsilon = 0.001$, $L = 1$, $x_0 = 1/2$. Inset corresponding to the maximum values of the distribution as a function of the normalized coupling strength g/ω_c.

In Figs. 10 and 11 the mean field profile given by (63) is computed squared and normalized by the coupling g/ω_c. It is done for $M = 30$ and $M = 1000$ respectively, in order to understand and better characterize the obtained curve for a lower number of modes in the first place, and then proceed with its behaviour in the maximum value of modes we are working with.

To further characterize the field, in the left inset in both figures the maximum values of the mean field profile is computed in terms of the normalized coupling strength g/ω_c, clearly observing a step function. In our extension to $M = 1000$ modes in Fig. 11 a curve resembling a Dirac-delta is obtained. As we can see in both figures, the curve converges at high values of

the coupling strength as soon as we increase it. Looking back at our equation for the field (63), we confirm that for large g/ω_c it reduces to

$$\langle E^+(x)\rangle \overset{g/\omega_c \gg 1}{=} \frac{g}{\omega_c} \sum_k \sin(k\pi x_0)\sin(k\pi x), \tag{65}$$

which depends only linearly on the g, which justifies the convergence for the field observed in both figures when plotting $\omega_c/g\langle E^+(x)\rangle$.

This leads us to an important observation. As we have computed the field in the GS of the system, we have obtained a macroscopic value for the electric field in the DSC exclusively due to the ultrastrong coupling of the TLS with the cavity, with no external excitation. A remarkable result because if we had a cavity without a TLS there would not be a macroscopic value of the field.

Conclusions

The outset of this Undergraduate Dissertation has included a discussion on previous theory regarding cavity QED and the importance of polaron transform as a semianalytical technique for solving problems with the paradigmatic spin-boson model.

Subsequently, we have proposed a new polaron *ansatz*, based on the inclusion of a parity breaking term given by a bias, and we have computed the transformed Hamiltonian of a spin-boson-like model in the polaron picture. When comparing our new polaron *ansatz* to a more typical realization of this approach we have found that the one proposed in this work showed a better performance describing the ground state of the system.

Thereupon, using this new transformation we have studied the phenomenology of the system in a wide range of coupling strengths covering the USC and DSC regimes, including the renormalization of the qubit frequency Δ_r and the bias ϵ_r, as well as the spin observables $\langle\sigma^x\rangle$, $\langle\sigma^z\rangle$ and P_e. We have achieved convergence for the studied parameters at a number of modes $M > 500$, identifying therefore a method to solve a system in the USC regime whose Hilbert space would be excessively large otherwise, but here without the need for approximations such as the RWA. Finally we have observed the existence of a macroscopic electric field inside the cavity for coupling regimes in the DSC, originating from the ultrastrong coupling between the cavity and the TLS in its ground state.

The benchmark offered by the multimode case opens a wide range of possibilities for further studies, considering that this has served as an introductory use case. For instance, this approach could also be applied to other models involving two level systems coupled to a set of electromagnetic modes such as in waveguide QED setups. Besides, we could generalize the Polaron transformation to multilevel systems.

References

[1] Antonio Acín et al. The quantum technologies roadmap: a european community view. *New Journal of Physics*, 20(8):080201, 2018.

[2] David Zueco. Light-matter interaction in the non-perturbative regime: a lecture. *Revista de la Real Academia de Ciencias, Zaragoza*, 171(74):41–74, 2019.

[3] Anton Frisk Kockum, Adam Miranowicz, Simone De Liberato, Salvatore Savasta, and Franco Nori. Ultrastrong coupling between light and matter. *Nature Review Physics*, 1(1):19–40, 2019.

[4] Carlos Sánchez Muñoz, Franco Nori, and Simone De Liberato. Resolution of superluminal signalling in non-perturbative cavity quantum electrodynamics. *Nature Communications*, 9(1), 2018.

[5] Robert Silbey and Robert A Harris. Variational calculation of the dynamics of a two level system interacting with a bath. *The Journal of Chemical Physics*, 80(6):2615–2617, 1984.

[6] Ulrich Weiss. *Quantum dissipative systems*. World Scientific, 2012.

[7] Isaac Fernando Quijandria Diaz. *One-dimensional bosons in circuit QED*. PhD thesis, Universidad de Zaragoza, 2015.

[8] Juan Román-Roche, Eduardo Sánchez-Burillo, and David Zueco. Bound states in ultrastrong waveguide QED. *Physical Review A*, 102(2), 2020.

[9] Alex W Chin, Javier Prior, Susana F Huelga, and Martin B Plenio. Generalized polaron ansatz for the ground state of the sub-ohmic spin-boson model: An analytic theory of the localization transition. *Physical Review Letters*, 107(16):160601, 2011.

[10] Hang Zheng, Zhiguo Lü, and Yang Zhao. Ansatz for the quantum phase transition in a dissipative two-qubit system. *Physical Review E*, 91:062115, 2015.

[11] Moein Malekakhlagh, Alexandru Petrescu, and Hakan E. Türeci. Cutoff-free circuit quantum electrodynamics. *Physical Review Letters*, 119(7), 2017.

A Calculations in the polaron treatment

A.1 Choice of $|S\rangle = |0\rangle$ as the corresponding to the ground state in original polaron treatment

If we know the matrix representation of σ^z and its eigenvectors $|\pm\rangle = \frac{1}{2}(|1\rangle \pm |0\rangle)$ (expressed as linear combinations of the eigenvectors of σ_x $|0\rangle$ and $|1\rangle$), so that $\sigma^z|\pm\rangle = \pm|\pm\rangle$, we can express the Spin vector as a linear combination of the eigenvectors of σ^z, so that $|S\rangle = \alpha|+\rangle + \beta|-\rangle$.

First of all, not having a GS with σ^x would imply

$$\begin{aligned}
&\langle\vec{0_k}|\langle S|\left(\frac{\Delta}{2}e^{2\sigma^z\sum_k(f_k b_k^+ - f_k b_k)}\right)|S\rangle|\vec{0_k}\rangle \\
&= \frac{\Delta}{2}\langle\vec{0_k}|\left(\alpha^*\langle+| + \beta^*\langle-|\right)\left(e^{2\sum_k(f_k b_k^+ - f_k b_k)}\right)\left(\alpha|+\rangle + \beta|+\rangle\right)|\vec{0_k}\rangle \\
&= \frac{\Delta}{2}\langle\vec{0_k}|\left(\alpha^*\langle+| + \beta^*\langle-|\right)\left(\alpha e^{2\sum_k(f_k b_k^+ - f_k b_k)}|+\rangle|\vec{0_k}\rangle + \beta e^{-2\sum_k(f_k b_k^+ - f_k b_k)}|-\rangle|\vec{0_k}\rangle\right) \\
&= \frac{\Delta}{2}\left(\langle\vec{0_k}||\alpha|^2 e^{2\sum_k(f_k b_k^+ - f_k b_k)}|\vec{0_k}\rangle + \langle\vec{0_k}||\beta|^2 e^{-2\sum_k(f_k b_k^+ - f_k b_k)}|\vec{0_k}\rangle\right) \\
&= \frac{\Delta}{2}\left(|\alpha|^2 e^{-2\sum_k|f_k|^2} + |\beta|^2 e^{-2\sum_k|f_k|^2}\right) = \frac{\Delta}{2}e^{-2\sum_k|f_k|^2} = \frac{\Delta_r}{2},
\end{aligned} \tag{66}$$

with the renormalized qubit frequency $\Delta_r = e^{-2\sum_k|f_k|^2}$.

If we substitute $|S\rangle$ in our real expression of the ground state energy (47), we now have a σ^z, so we should express first $|S\rangle$ in terms of its eigenvectors in order to operate with it, so that $|S\rangle = \alpha|0\rangle + \beta|0\rangle$, knowing $\sigma^x|0\rangle = -|0\rangle$ and $\sigma^x|1\rangle = +|1\rangle$. Taken all of this into account we obtain

$$\begin{aligned}
E_{GS} &= \langle\vec{0_k}|\langle S|\left(\frac{\Delta}{2}e^{2\sigma^z\sum_k(f_k b_k^+ - f_k b_k)}\sigma^x\right)|S\rangle|\vec{0_k}\rangle \\
&= \frac{\Delta}{2}\langle\vec{0_k}|\left(\alpha^*\langle0| + \beta^*\langle1|\right)\left(e^{2\sigma^z\sum_k(f_k b_k^+ - f_k b_k)}\sigma^x\right)\left(\alpha|0\rangle + \beta|1\rangle\right)|\vec{0_k}\rangle \\
&= \frac{\Delta}{2}\langle\vec{0_k}|\left(\alpha^*\langle0| + \beta^*\langle1|\right)\left(e^{2\sigma^z\sum_k(f_k b_k^+ - f_k b_k)}\right)\left(-\alpha|0\rangle + \beta|1\rangle\right)|\vec{0_k}\rangle\,.
\end{aligned} \tag{67}$$

Now we have to express again everything in terms of the eigenvectors of σ^z in order to operate with it, that is,

$$\begin{aligned}
|S\rangle &= \alpha|0\rangle + \beta|1\rangle = \alpha\left(\frac{1}{\sqrt{2}}(|+\rangle + |-\rangle\right) + \beta\left(\frac{1}{\sqrt{2}}(|+\rangle - |-\rangle\right) \\
&= \left(\frac{\alpha+\beta}{\sqrt{2}}\right)|+\rangle + \left(\frac{\alpha-\beta}{\sqrt{2}}\right)|-\rangle\,,
\end{aligned} \tag{68}$$

$$\begin{aligned}
\sigma^x|S\rangle &= -\alpha|0\rangle + \beta|1\rangle = -\alpha\left(\frac{1}{\sqrt{2}}(|+\rangle + |-\rangle)\right) + \beta\left(\frac{1}{\sqrt{2}}(|+\rangle - |-\rangle)\right) \\
&= \left(\frac{\beta-\alpha}{\sqrt{2}}\right)|+\rangle - \left(\frac{\alpha+\beta}{\sqrt{2}}\right)|-\rangle\,.
\end{aligned} \tag{69}$$

And finally we can get an expression for E_{GS} (67), which is

$$
\begin{aligned}
E_{GS} = \frac{\Delta}{2}\langle\vec{0_k}| \left[\left(\frac{\alpha^*+\beta^*}{\sqrt{2}}\right)\langle+| + \left(\frac{\alpha^*-\beta^*}{\sqrt{2}}\right)\langle-|\right]\left(e^{2\sigma^z\sum_k(f_k b_k^+ - f_k b_k)}\right)\cdot \\
\cdot\left[\left(\frac{\beta-\alpha}{\sqrt{2}}\right)|+\rangle - \left(\frac{\alpha+\beta}{\sqrt{2}}\right)|-\rangle\right]|\vec{0_k}\rangle \\
= \frac{\Delta}{4}(\alpha^*+\beta^*)(\beta-\alpha)\langle\vec{0_k}|\left(e^{2\sum_k(f_k b_k^+ - f_k b_k)}\right)|\vec{0_k}\rangle \\
- \frac{\Delta}{4}(\alpha^*-\beta^*)(\alpha+\beta)\langle\vec{0_k}|\left(e^{-2\sum_k(f_k b_k^+ - f_k b_k)}\right)|\vec{0_k}\rangle \\
= \frac{\Delta}{4}(\alpha^*+\beta^*)(\beta-\alpha)\langle\vec{0_k}|\left(e^{-2\sum_k|f_k|^2}\right)|\vec{0_k}\rangle \\
- \frac{\Delta}{4}(\alpha^*-\beta^*)(\alpha+\beta)\langle\vec{0_k}|\left(e^{-2\sum_k|f_k|^2}\right)|\vec{0_k}\rangle \\
= \frac{\Delta_r}{4}\left[(\alpha^*+\beta^*)(\beta-\alpha) - (\alpha^*-\beta^*)(\alpha+\beta)\right] \\
= \frac{\Delta_r}{2}Re\left[(\alpha^*+\beta^*)(\beta-\alpha)\right] = \frac{\Delta_r}{2}\left(-|\alpha|^2+|\beta|^2\right)
\end{aligned} \tag{70}
$$

If we want this to be minimum (we want the ground state), α has to be maximum, so $\alpha = 1$ and $\beta = 0$ and thus our GS is $|S\rangle = |0\rangle$.

A.2 Derivation of the commutation relations

If we name some operators A, B, and C such that

$$[B, A] = C. \tag{71}$$

Then, if

$$[C, A] = 0, \tag{72}$$

it follows that

$$[B, A^n] = nCA^{n-1}. \tag{73}$$

From this it can be proven

$$\left[B, e^A\right] = Ce^A. \tag{74}$$

We can prove this easily as follows. Firstly we prove (73) so that

$$
\begin{aligned}
[B, A^n] = [B, AA^{n-1}] = A[B, A^{n-1}] + [B, A]A^{n-a} \overset{(73)}{=} A(n-1)CA^{n-2} + CA^{n-1} \\
\overset{(72)}{=} (n-1)CA^{n-1} + CA^{n-1} = nCA^{n-1}.
\end{aligned} \tag{75}
$$

Secondly, (74) can be proven with

$$
\begin{aligned}
[B, e^A] = \sum_{n=0}\frac{[B, A^n]^n}{n!} = [A, \mathbb{1}] + \sum_{n=1}\frac{[B, A^n]^n}{n!} = \sum_{n=1}\frac{nCA^{n-1}}{n!} \\
= C\sum_{n=1}\frac{A^{n-1}}{(n-1)!} = C\sum_{n=0}\frac{A^n}{n!} = Ce^A.
\end{aligned} \tag{76}
$$

Now, talking already for our case, fordemonstrating the first expression (16), that is, $[b_k, U_Z] = \pm\sigma^z f_k U_Z$, we assume $A \equiv \pm\sigma^z\hat{\alpha}$, $B \equiv b_k$ and $C \equiv \pm\sigma^z f_k$, proving (71) as

$$[b_k, \pm\sigma^z\hat{\alpha}] = \pm\sigma^z f_k \left([b_k, b_k^\dagger] + [b_k, -b_{k'}]\right) = \pm\sigma^z f_k. \tag{77}$$

Moreover, $[\pm\sigma^z f_k, \pm\sigma^z\hat{\alpha}] = 0$ (72) and thus (73) holds, proving (74)

$$[b_k, e^{\pm\sigma^z\hat{\alpha}}] = \pm\sigma^z f_k U_Z. \tag{78}$$

Then for demonstrating the second expression (17), that is, $[b_k, U_{\mathbb{1}}] = \pm l_k U_{\mathbb{1}}$, naming $A \equiv \pm\hat{\beta}$, $B \equiv b_k$ and $C = \pm l_k$ we follow the same procedure, leaving

$$[b_k, \pm\hat{\beta}] = \pm l_k \left([b_k, b_k^\dagger] + [b_k, -b_{k'}]\right) = \pm l_k, \tag{79}$$

$$[\pm l_k, \pm\hat{\beta}] = 0, \tag{80}$$

$$[b_k, e^{\pm\hat{\beta}}] = \pm l_k U_{\mathbb{1}}, \tag{81}$$

fulfilling all the already mentioned conditions.

A.3 Obtention of the effective Hamiltonians in polaron picture

In this section we compute the $\mathcal{H}_{\text{eff}}$ for both parameterizations with (46) as the starting point of our calculations, that is,

$$\begin{aligned}\mathcal{H}_P = \frac{W_r}{2}\sigma^x + \sum_k \omega_k b_k^\dagger b_k + \sum_k \omega_k l_k \left(b_k^\dagger + b_k\right) - \Delta_r\sigma^z\sigma^x \sum_k f_k \left(b_k^\dagger - b_k\right) \\ + (\cos\theta\sigma^z + \sin\theta\sigma^x)\sum_k (c_k + \omega_k f_k)\left(b_k^\dagger + b_k\right) + 2\sum_k c_k f_k + \sum_k \omega_k \left(f_k^2 + l_k^2\right)\end{aligned}$$

We start with the first parameterization. Matching the coefficients from $\sigma^z(b_k^\dagger + b_k)$ and $\sigma^z\sigma^x(b_k^\dagger - b_k)$ and using (48) and (49) we obtain

$$\cos\theta\,(c_k + \omega_k f_k) = -\Delta_r f_k \iff \xi_k = -\frac{\omega_k}{W_r + \omega_k} \implies f_k = -\frac{c_k}{W_r + \omega_k}. \tag{82}$$

Using the same procedure for the coefficients from $\sigma^x(b_k^\dagger + b_k)$ and $(b_k^\dagger + b_k)$ it leaves

$$\sin\theta\,(c_k + \omega_k f_k) = \omega_k l_k \iff \lambda_k = \frac{\epsilon_r}{W_r + \omega_k} \implies l_k = \frac{c_k}{\omega_k}\frac{\epsilon_r}{W_r + \omega_k}. \tag{83}$$

Now we substitute our new expressions for the variational parameters in $\mathcal{H}_P$. Computing f_k given by (82) leaves

$$\begin{aligned}&\cos\theta\sigma^z \sum_k (c_k + \omega_k f_k)\left(b_k^\dagger + b_k\right) - \Delta_r\sigma^z\sigma^x \sum_k f_k \left(b_k^\dagger - b_k\right) \\ &= -\sum_k \Delta_r f_k \left[\sigma^z\sigma^x\left(b_k^\dagger - b_k\right) + \sigma^z\left(b_k^\dagger + b_k\right)\right] \\ &= -\sum_k \Delta_r f_k \left[b_k^\dagger \underbrace{(\sigma^z + \sigma^z\sigma^x)}_{2\sigma^-} + b_k \underbrace{(\sigma^z - \sigma^z\sigma^x)}_{2\sigma^+}\right]\end{aligned}$$

$$= -2\Delta_r \sum_k f_k \left(\sigma^- b_k^\dagger + \sigma^+ b_k\right), \tag{84}$$

having used

$$\sigma^z + \sigma^z\sigma^x = 2\sigma^-,$$
$$\sigma^z - \sigma^z\sigma^x = 2\sigma^+.$$

Besides, computing l_k given by (83) results in

$$\sin\theta\sigma^x \sum_k (c_k + \omega_k f_k)\left(b_k^\dagger + b_k\right) + \sum_k \omega_k l_k \left(b_k^\dagger + b_k\right) = (\sigma^x + \mathbb{1}) \sum_k \omega_k l_k \left(b_k^\dagger + b_k\right) \tag{85}$$

Finally, substituting (84) and (85) leaves the final expression of the effective transformed Hamiltonian for our first parameterization (50), that is,

$$\begin{aligned}(\mathcal{H}_{\text{eff},1})_P = \frac{W_r}{2}\sigma^x + \sum_k \omega_k b_k^\dagger b_k + (\sigma^x + \mathbb{1}) \sum_k \omega_k l_k \left(b_k^\dagger + b_k\right) \\ - 2\Delta_r \sum_k f_k \left(\sigma^- b_k^\dagger + \sigma^+ b_k\right) + 2\sum_k c_k f_k + \sum_k \omega_k \left(f_k^2 + l_k^2\right).\end{aligned} \tag{86}$$

Now we turn the scope to the second parameterization. Trying to compute a variation of the first one we can just compute the variational parameters given by (53) and (54), that is,

$$f_k = -\frac{c_k}{\omega_k}, \tag{87}$$
$$l_k = 0. \tag{88}$$

Substituting directly in the transformed Hamiltonian (46) the problematic term vanish, leaving (52), with the form

$$(\mathcal{H}_{\text{eff},2})_P = \frac{W_r}{2}\sigma^x + \sum_k \omega_k b_k^\dagger b_k - \Delta_r \sigma^z\sigma^x \sum_k f_k \left(b_k^\dagger - b_k\right) + 2\sum_k c_k f_k + \sum_k \omega_k f_k^2. \tag{89}$$

B Code

All numerical calculations performed for this Undergraduate Dissertation were based on proprietary code developed by the author that can be found here.